CFD Modeling for Selective Formation of Propylene from Methanol Over Synthesized Mn-Substituted MFI Metallosilicate Catalyst

N. Hadi [1], A. Niaei [2], R. Alizadeh [1*]

[1] *Faculty of Chemical Engineering, Sahand University of Technology, Tabriz, Iran*
[2] *Faculty of Chemical Engineering, University of Tabriz, Tabriz, Iran*

ARTICLE INFO	ABSTRACT
	The high silica Mn-substituted MFI metallosilicate catalyst with Si/Al molar ratio of 220 and Si/Mn molar ratio of 50 was successfully synthesized by hydrothermal method. The catalyst sample was appropriately characterized by XRD, FE-SEM, EDX, and BET techniques. The Mn-substituted MFI metallosilicate has not been reported as the potential catalyst for methanol-to-propylene (MTP) reaction. The prepared catalyst was examined in the MTP reaction in the optimal operating conditions. Furthermore, to elucidate the flow field of the MTP fixed bed reactor, a three-dimensional (3D) reactor model was developed. A detailed reaction mechanism that was proposed for the MTP reaction over the Mn-impregnated MFI zeolite (Mn/H-ZSM-5) was properly employed. The reaction mechanism was integrated to a computational fluid dynamics (CFD) for simulating kinetics, energy equation, and the hydrodynamics of the MTP process, simultaneously. The component distribution during the implementation of the MTP reaction was also simulated as a function of time on stream. The CFD modeling results were validated by the actual data obtained over the Mn-substituted MFI metallosilicate catalyst. With regard to the findings, the experimental data were in good agreement with the predicted values of the CFD modeling.

1. Introduction

Propylene is one of the important monomers in petrochemical industry. In recent years, due to an increase in universal demand for propylene, the conventional processes, such as steam cracking and fluidized catalytic cracking (FCC) of crude oil, cannot afford to supply the required propylene. The catalytic conversion of methanol to propylene (MTP) process, which was initiated from the methanol to olefins (MTO) process, was launched for selective production of propylene form low-priced alcohol (methanol) [1]. The MTP process is usually applied to the MFI-type zeolite catalysts [2]. Some investigations were conducted to modify the MFI zeolites and utilize them in the MTP reaction. For instance, Hadi et al. improved the activity of the MFI zeolite catalyst known as H-ZSM-5 by impregnation of Ca, Mn, Cr, Fe, Ni, Ag, Ce, and P [3]. The best selectivity of propylene was acquired

with respect to the Mn/H-ZSM-5 catalyst. Rostamizadeh and Taeb synthesized and impregnated the high silica H-ZSM-5 catalyst with Si/Al ratio of 200 using different promoters including P, Mn, Mg, and Cs [4]. Among the modified catalysts, the highest methanol conversion was demonstrated by the Mn/H-ZSM-5 and P/H-ZSM-5 catalysts. Also, the highest propylene selectivity was represented by the Mn/H-ZSM-5 catalyst.

Few studies on the reactor modeling, especially on the computational fluid dynamics (CFD) of the MTO/MTP, were found in the literature. For instance, Guo et al. [5, 6] carried out some experiments using the monolithic and packed bed reactors for the MTP. Simulation results demonstrated that the monolithic reactor significantly enhanced the methanol conversion and propylene selectivity. Alwahabi and Froment [7] designed various types of reactors such as fixed bed reactors, e.g., multi-tubular and quasi-isothermal or multi-bed adiabatic reactors, for the MTO reaction. Modeling the reactors for each type of the reactor led to the optimal operation conditions, while the flow regime of the various reactor types was not studied. Schoenfelder et al. [8] designed a circulating, fluidized bed reactor (CFB) for the MTO. Based on the estimated kinetic parameters, methanol conversion, and product distribution investigated on the CFB reactor, Soundararajan et al. [9] modeled numerically the MTO reactor in a CFB reactor. Modeling the reactor demonstrated that the selectivity of ethylene and propylene decreased by increasing coke deposition on the catalyst.

Detailed experimental investigations of the MTO/MTP reactions have recently attracted a considerable amount of researches due to the process's complex hydrodynamics, kinetics, and reaction mechanism. CFD provides a useful tool to delve into these complexities [10]. A two-dimensional reactor model was developed by Zhuang et al. [11] to simulate the flow regime in a fixed bed reactor for the MTO over SAPO-34 catalyst. A kinetic model based on a lumped-species reaction mechanism was employed. The product distribution was obtained as a function of the feed temperature and the space velocity of feed. Forr the MTO reaction, Chang et al. [10] presented a computational research of the hydrodynamics and lumped-species kinetic reactions in a fluidized bed reactor (FBR). The results indicated that methanol conversion and product yields were more sensitive to the reaction temperature than to the initial methanol content in the feed. Zhu et al. [12] developed a filtered two-fluid model to describe the gas-solid flow behavior in a large scale FBR for the MTO reaction. They indicated that as the size of catalyst particles decreases, the clustering phenomena near the wall regions become more obvious. Lu et al. [13] tried to integrate the classic chemical reaction engineering model with CFD in order to speed up the calculations. The continuous stirred tank reactor (CSTR) model was established to estimate the steady-state distribution of coke content. It was set as the initial distribution for CFD simulation to shorten the calculation time.

The main disadvantages of the fluidized bed reactors are as follows: the low single pass conversion of methanol, the high operating costs, and considerable catalyst attrition [7]. Due to the mentioned limitations, scaling up the MTP/MTO process in the FBR is a hard work. Comparatively, the design of the fixed bed reactor is rather inexpensive and simple, and controlling its operating conditions is relatively easy. It also plays a key role in the industrial chemistry [14]. Considering the

other processes besides the MTO/MTP, researchers have allocated notable attention to the CFD approach in the fixed bed reactors [14-20]. Nijemeisland and Dixon [14] investigated the flow behavior and the wall heat flux in a packed bed of spheres. Guardo et al. [20] studied particles to measure the fluid heat transfer in fixed beds employing a CFD based on the Eulerian-Eulerian approach. Salari et al. [18] utilized the CFD modeling to analyze the fixed bed reactor of catalytic cracking of naphtha based on the Eulerian relations. Shahhosseini et al. [19] simulated gas to liquids (GTL) process in a catalytic fixed bed reactor by utilizing a two-dimensional CFD approach. As mentioned above, CFD modeling of the MTO/MTP reactions using the lumped kinetic models has been extensively reported in the literature. However, employing a detailed reaction network in a fixed bed reactor for CFD modeling is lacking.

In the current investigation, the Mn-substituted MFI metallosilicate (H-MnAlMFI) was synthesized by hydrothermal method. The prepared catalyst was examined in the fixed bed reactor of the MTP reaction in the optimal operating conditions. A three-dimensional CFD model was developed for the fixed bed MTP reactor. The CFD modeling was integrated with a detailed kinetic model. It should be mentioned that the kinetic model was adopted from our previous work [3]. The flow regime, profiles of chemical species, and temperature profile of the reactor were appropriately determined, using the CFD modeling. Finally, a comparison between the experimental values of chemical species and the predicted data of the CFD modeling was accomplished.

2. Experimental

2.1. Materials
The starting materials were tetraethyl ortho silicate (99 wt %), sodium hydroxide (98 wt %), aluminum sulphate (98 wt %), manganese (II) nitrate ($Mn(NO_3)_2.4H_2O$, 98 wt %), ammonium chloride (98 wt %), ammonium fluoride (98 wt %), and tetra propyl ammonium bromide (99 wt %). All of these materials were extra pure supplied by Merck and Aldrich companies.

2.2. Catalyst synthesis
The Mn-substituted MFI metallosilicate (H-MnAlMFI) was synthesized by hydrothermal method. The synthetic gel was prepared by molar composition of 100 SiO_2: 0.2273 Al_2O_3: 2 MnO: 18.9 Na_2O: 20.5 NH_4F: 12.5 TPAB: 3200 H_2O. The aim was to reach Na-MnAlMFI with the Si/Al ratio of 220 and the Si/Mn ratio of 50. The method advised by Jin et al. [21] was used as a model for the method of gel preparing . For hydrothermal synthesis, the gel was transferred to the Teflon-lined stainless-steel autoclave at 170 °C for 72 h. Finally, the Na-MnAlMFI was converted to H-MnAlMFI catalyst by ion exchange method. The sample in the NH_4-form was prepared by a 1 $mol.L^{-1}$ ammonium chloride solution at 50 °C for 48 h agitation. The H-MnAlMFI catalyst was acquired through drying and calcination of the NH_4-form of MFI zeolite in atmospheric air at 100 °C for 12 h and 500 °C for 6 h, respectively.

2.3. Catalyst characterization techniques
The structure of H-MnAlMFI catalyst was determined by powder X-ray diffraction (XRD) by a Siemens® D500 X-ray diffractometer. In order to specify the surface morphology of the catalyst sample, field emission scanning electron microscopy (FE-SEM) was used. The FE-SEM images were

taken by a MIRA3 TESCAN® microscope. The qualitative elemental analysis of the catalyst sample was performed by energy dispersive X-ray (EDX) technique.

2.4. Process set up for catalyst examinations

The examinations of catalyst evaluation were conducted under the atmospheric pressure in a fixed bed reactor. The operating conditions were regulated at their optimal values according to the literature review [4, 22-24]. The operating conditions of the MTP reaction were as follows: reaction temperature of 500 °C, methanol weight hourly space velocity (WHSV) of 2.5 h^{-1}, and methanol molar ratio in the feedstock of 50 %. The products of the MTP reaction were analyzed by Shimadzu's GC-2010 Plus. The schematic flow diagram of the experimental setup is illustrated in Fig. 1.
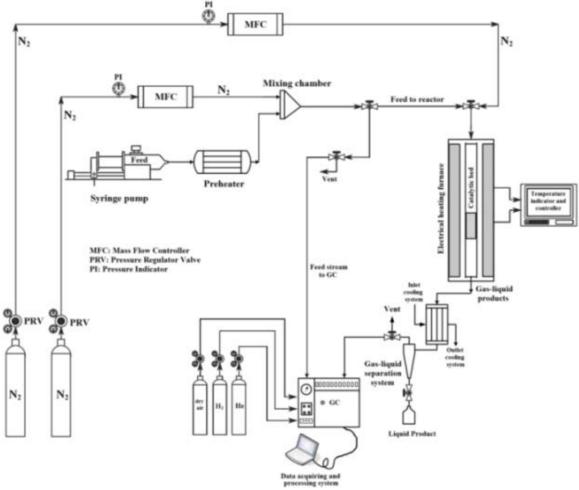

Figure 1. The experimental setup for catalyst examinations in methanol to propylene process.

3. The CFD approach

The model treats the flow hydrodynamics, the temperature profile, and distribution of chemical species in the experimental MTP reactor over heterogeneous catalysis (H-MnAlMFI). The model incorporated the free and porous media flow in the fixed bed and plug flow reactor. The catalytic bed was assumed as a continuous porous medium. The reaction mechanism and kinetic model were inspired from our previous work [3] proposed over the Mn/H-ZSM-5 catalyst. Table 1 tabulates the reaction mechanism and kinetic model.

Table 1
The reaction mechanism and the kinetic expressions proposed by Hadi et al. [3] used for CFD modeling.

Reaction mechanism	Differential equations of chemical species	Modified Arrhenius equations (h^{-1}) $T_m = 475\ °C$
	$\frac{d\omega_{MeOH}}{d(W/F_{MeOH})} = -(4r_1 + 5r_2 + 6r_3 + 7r_4 + r_5 + r_6 + r_7 + 2r_{12})$	$k_1 = 0.86 \times \exp\left[\frac{-9560}{R}\left(\frac{1}{T} - \frac{1}{T_m}\right)\right]$
	$\frac{d\omega_{C_2H_4}}{d(W/F_{MeOH})} = 3r_9 + r_{10}$	$k_2 = 0.21 \times \exp\left[\frac{-10620}{R}\left(\frac{1}{T} - \frac{1}{T_m}\right)\right]$
	$\frac{d\omega_{C_3H_6}}{d(W/F_{MeOH})} = 2r_8 + r_{11}$	$k_3 = 3.28 \times \exp\left[\frac{-10300}{R}\left(\frac{1}{T} - \frac{1}{T_m}\right)\right]$
$4\,CH_3OH \xrightarrow{k_1} C_4H_8 + 4\,H_2O$		
$5\,CH_3OH \xrightarrow{k_2} C_5H_{10} + 5\,H_2O$	$\frac{d\omega_{C_4H_8}}{d(W/F_{MeOH})} = r_1 - r_5 + r_{10} + r_{11}$	$k_4 = 2.39 \times \exp\left[\frac{-8040}{R}\left(\frac{1}{T} - \frac{1}{T_m}\right)\right]$
$6\,CH_3OH \xrightarrow{k_3} C_6H_{12} + 6\,H_2O$		
$7\,CH_3OH \xrightarrow{k_4} C_7H_{14} + 7\,H_2O$	$\frac{d\omega_{C_5H_{10}}}{d(W/F_{MeOH})} = r_2 + r_5 - r_6$	$k_5 = 0.69 \times \exp\left[\frac{-10030}{R}\left(\frac{1}{T} - \frac{1}{T_m}\right)\right]$
$CH_3OH + C_4H_8 \xrightarrow{k_5} C_5H_{10} + H_2O$		
$CH_3OH + C_5H_{10} \xrightarrow{k_6} C_6H_{12} + H_2O$	$\frac{d\omega_{CH_4}}{d(W/F_{MeOH})} = r_{12}$	$k_6 = 1.66 \times \exp\left[\frac{-7960}{R}\left(\frac{1}{T} - \frac{1}{T_m}\right)\right]$
$CH_3OH + C_6H_{12} \xrightarrow{k_7} C_7H_{14} + H_2O$		$k_7 = 1.40 \times \exp\left[\frac{-10860}{R}\left(\frac{1}{T} - \frac{1}{T_m}\right)\right]$
$C_6H_{12} \xrightarrow{k_8} 2\,C_3H_6$	$\frac{d\omega_{C_2H_6}}{d(W/F_{MeOH})} = r_{13}$	$k_8 = 2.65 \times \exp\left[\frac{-11370}{R}\left(\frac{1}{T} - \frac{1}{T_m}\right)\right]$
$C_6H_{12} \xrightarrow{k_9} 3\,C_2H_4$		
$C_6H_{12} \xrightarrow{k_{10}} C_2H_4 + C_4H_8$	$\frac{d\omega_{C_3H_8}}{d(W/F_{MeOH})} = r_{14}$	$k_9 = 0.69 \times \exp\left[\frac{-11250}{R}\left(\frac{1}{T} - \frac{1}{T_m}\right)\right]$
$C_7H_{14} \xrightarrow{k_{11}} C_3H_6 + C_4H_8$		$k_{10} = 0.48 \times \exp\left[\frac{-11180}{R}\left(\frac{1}{T} - \frac{1}{T_m}\right)\right]$
$2\,CH_3OH \xrightarrow{k_{12}} CH_4 + Coke + H_2O$	$\frac{d\omega_{C_4H_{10}}}{d(W/F_{MeOH})} = r_{15}$	$k_{11} = 2.46 \times \exp\left[\frac{-10200}{R}\left(\frac{1}{T} - \frac{1}{T_m}\right)\right]$
	$\frac{d\omega_{C_5H_{12}}}{d(W/F_{MeOH})} = r_{16}$	$k_{12} = 0.23 \times \exp\left[\frac{-10880}{R}\left(\frac{1}{T} - \frac{1}{T_m}\right)\right]$
$C_7H_{14} \longrightarrow$ Alkanes $\begin{cases} \xrightarrow{k_{13}} C_2H_6 \\ \xrightarrow{k_{14}} C_3H_8 \\ \xrightarrow{k_{15}} C_4H_{10} \\ \xrightarrow{k_{16}} C_5H_{12} \end{cases}$	$\frac{d\omega_{Aromatics}}{d(W/F_{MeOH})} = r_{17}$	$k_{13} = 0.39 \times \exp\left[\frac{-10720}{R}\left(\frac{1}{T} - \frac{1}{T_m}\right)\right]$
		$k_{14} = 0.95 \times \exp\left[\frac{-13630}{R}\left(\frac{1}{T} - \frac{1}{T_m}\right)\right]$
	$\frac{d\omega_{Coke}}{d(W/F_{MeOH})} = r_{12}$	$k_{15} = 2.25 \times \exp\left[\frac{-9450}{R}\left(\frac{1}{T} - \frac{1}{T_m}\right)\right]$
$C_7H_{14} \xrightarrow{k_{17}}$ Aromatics		$k_{16} = 1.63 \times \exp\left[\frac{-10700}{R}\left(\frac{1}{T} - \frac{1}{T_m}\right)\right]$
	$\frac{d\omega_{C_6H_{12}}}{d(W/F_{MeOH})} = r_3 + r_6 - r_7 - r_8 - r_9 - r_{10}$	$k_{17} = 1.63 \times \exp\left[\frac{-12410}{R}\left(\frac{1}{T} - \frac{1}{T_m}\right)\right]$
	$\frac{d\omega_{C_7H_{14}}}{d(W/F_{MeOH})} = r_4 + r_7 - r_{11} - r_{13} - r_{14} - r_{15} - r_{16} - r_{17}$	

3.1. Model definition

The reactor includes a tubular structure. The incoming chemical species (methanol) in the reaction section reacted on a fixed and porous catalytic bed. The model integrated the free fluid flow and porous media flow through the Navier-Stokes relations and Brinkman's extension of Darcy's law. It was assumed that the porous medium was a chemically inert material. Due to symmetry, it was required to model only half of the reactor. The time-dependent Navier-Stokes equation, which was described the fluid flow, is considered according to Equation 1.

$$\rho\frac{\partial \mathbf{u}}{\partial t} + \rho(\mathbf{u}.\nabla)\mathbf{u} = \nabla.[-p\mathbf{I} + \mu(\nabla\mathbf{u} + (\nabla\mathbf{u})^T)] + \mathbf{F} \tag{1}$$

The gas phase continuity equation, which should be solved with Equation 1, is as follows:

$$\frac{\partial \rho_g}{\partial t} + \nabla.(\rho_g\mathbf{u}) = 0 \tag{2}$$

The gas stream was assumed as incompressible flow; therefore, Equation 2 was simplified to Equation 3.

$$\nabla.\mathbf{u} = 0 \tag{3}$$

In the porous media, the Brinkman's extension of Darcy's law was used (Equation 4).

$$\frac{\rho}{\varepsilon_p}\left(\frac{\partial \mathbf{u}}{\partial t} + (\mathbf{u}.\nabla)\frac{\mathbf{u}}{\varepsilon_p}\right) = \nabla.\left[-p\mathbf{I} + \frac{\mu}{\varepsilon_p}\left(\nabla\mathbf{u} + (\nabla\mathbf{u})^T\right) - \frac{2\mu}{3\varepsilon_p}(\nabla.\mathbf{u})\mathbf{I}\right] - \frac{\mu}{\kappa_{br}}\mathbf{u} \qquad (4)$$

where μ denotes the dynamic viscosity of the fluid (kg.m^{-1}.s^{-1}), ε_p is the porosity (dimensionless), $\mathbf{u}$ the velocity vector (m.s^{-1}), ρ is the density (kg.m^{-3}), p is the pressure (Pa), and κ_{br} is the permeability (m^2). Since the feed contained the volumetric flow of 3600 (cm^3.h^{-1}) of N$_2$ inert gas with methanol WHSV (weight hourly space velocity) of 2.5 h^{-1}, it was assumed that the chemical species (both of the reactant and products) were in low concentrations compared to the carrier gas. In other words, the Fickian approach for the diffusion term in the mass transport can be applied. The mass transport for the components can be modeled by the convection-diffusion equation as follows:

$$\frac{\partial \omega_i}{\partial t} + \nabla.(-D_i\nabla\omega_i + \omega_i\mathbf{u}) = R_i \qquad (5)$$

where ω_i indicates the weight fraction of the ith species (dimensionless), D_i is the coefficient of diffusion (m^2.s^{-1}), and R_i is the reaction rate for the ith species ($g_i.h^{-1}g_{Catalyst}^{-1}$).

The gas phase stress-strain tensor can be evaluated as follows:

$$\boldsymbol{\tau} = \mu\left[\left(\nabla\mathbf{u} + (\nabla\mathbf{u})^T\right) - \frac{2}{3}(\nabla.\mathbf{u})\mathbf{I}\right] \qquad (6)$$

The energy balance of the reactor is given by:

$$\sum_i F_i C_{p,i}\frac{dT}{dV} = Q_{ext.} + Q \qquad (7)$$

where F_i is the molar flow rate of chemical species (mol.s^{-1}), V is the reactor volume (m^3), and $C_{p,i}$ is the molar heat capacity of chemical species (J.mol^{-1}.K^{-1}). $Q_{ext.}$ indicates the external heat added to or removed from the reactor. Q represents the heat of the chemical reactions (J.m^{-3}.s^{-1}).

$$Q = -\sum_j H_j r_j \qquad (8)$$

where H_j denotes the enthalpy of the jth reaction. The chemical reaction relations, the kinetic parameters, the thermodynamic properties of chemical species, and the feed molar rate should be provided as inputs of the energy balance equation. The thermodynamic properties of the chemical species are determined by utilizing the following polynomial expressions:

$$C_{p,i} = R(a_1 + a_2T + a_3T^2 + a_4T^3 + a_5T^4) \qquad (9)$$

$$h_i = R\left(a_1T + \frac{a_2}{2}T^2 + \frac{a_3}{3}T^3 + \frac{a_4}{4}T^4 + \frac{a_5}{5}T^5 + a_6\right) \qquad (10)$$

$$s_i = R\left(a_1\ln T + a_2T + \frac{a_3}{2}T^2 + \frac{a_4}{3}T^3 + \frac{a_5}{4}T^4 + a_7\right) \qquad (11)$$

where T shows the temperature (K), R is the gas constant: 8.314 (J.mol^{-1}.K^{-1}), h_i is the molar enthalpy of the chemical species (J.mol^{-1}), and s_i is the molar entropy of the chemical species (J.mol^{-1}.K^{-1}). A set of seven coefficients for each chemical species is required to input in the polynomial equations of 9, 10, and 11. Coefficients a_1 to a_5 are related to the heat capacity of the chemical species; coefficient a_6 is associated with the enthalpy of formation at 0 (K), and coefficient a_7 is related to the entropy of formation at 0 (K). The format of the polynomial equations is well appointed, one of which is referred to as CHEMKIN® or NASA. Based on the inlet boundary conditions, the velocity distribution and the evolution of weight fraction of chemical species can be determined. The inlet pressure of the reactor was adjusted at 101330 Pa. The no-slip boundary condition was considered for the internal wall of the reactor. The reactor was assumed to be an adiabatic

one with the reaction temperature of 500 °C (773.15 K) similar to the experimental value. The dominant equations were discretized in a non-uniform normal-sized mesh.

4. Results and discussion
4.1. Catalyst characterizations
The structure of the Mn-substituted MFI metallosilicate was elucidated by the XRD pattern. For comparison, the structure of the referenced conventional H-ZSM-5 was also investigated by the XRD (Fig. 2). The XRD analyses showed two individual sharp peaks at 2θ of 8-10° and 20-25°. Both of these sharp peaks corresponded with the referenced MFI type zeolite with respect to the JCPDS (Joint Committee on Powder Diffraction Standards) data [25]. According to the structure of referenced conventional H-ZSM-5, no considerable change in phase was detected in structure of the Mn-substituted MFI metallosilicate.
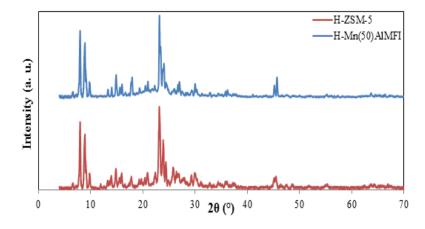

Figure 2. The XRD patterns of the conventional H-ZSM-5 and Mn-substituted MFI metallosilicate with Si/Mn molar ratio of 50 (H-Mn(50)AlMFI).

FE-SEM images displayed the surface morphology of the Mn-substituted MFI metallosilicate with Si/Mn molar ratio of 50 (Fig. 3). The FE-SEM images confirmed that the catalyst sample was comprised of the uniform particle sizes with identical shapes of the H-MnAlMFI aggregates. The total specific surface area (S_{BET}) of the catalyst sample is about 310.2 ($m^2.g^{-1}$).
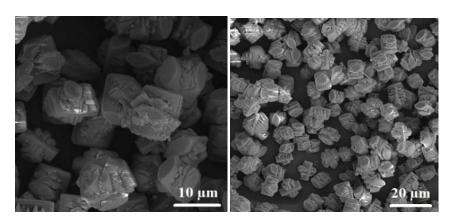

Figure 3. The FE-SEM images of the Mn-substituted MFI metallosilicate with Si/Mn molar ratio of 50 (H-Mn(50)AlMFI).

To investigate the presence of the required chemical species in the framework of the catalyst sample, the qualitative elemental analysis was accomplished by means of EDX analysis. Fig. 4 exhibits the EDX graph of the H-MnAlMFI catalyst. According to EDX graph, the peaks of the heteroatom of Mn were identified.
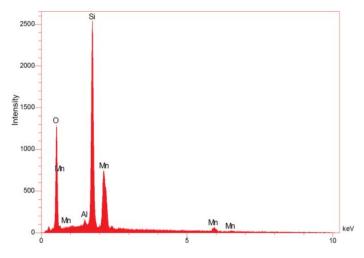

Figure 4. The EDX graph of the Mn-substituted MFI metallosilicate with Si/Mn molar ratio of 50 (H-Mn(50)AlMFI).

4.2. Model validation

The MTP reaction was conducted on the H-MnAlMFI catalyst with reaction temperature of 500 °C, methanol molar ratio in the feedstock of 50 %, and methanol WHSV of 2.5 h^{-1}. The above-mentioned operating conditions were also used for the CFD modeling of the MTP reactor. The CFD model was used to predict the dynamic changes of the chemical species besides the temperature profile of the reactor and also to investigate the hydrodynamic of the reacting flow. It is of note that although the kinetics and CFD modeling were carried out for a lab scale reactor, the findings can be employed for a large scale reactor due to the few effects of the reactor scale on the bulk reaction mechanism. The comparison between the experimental values and the predicted data of the CFD modeling is reported in Table 2, demonstrating that the experimental values sufficiently validated the model predicted data.

Table 2

Comparison of weight fractions of different products between CFD predicted data and experimental values at a reaction temperature of 500 °C, WHSV of 2.5 h^{-1} , and methanol molar ratio in feedstock of 50 % over H-MnAlMFI catalyst.

Weight percent	Methanol	Ethane	Ethylene	Propane	Propylene	Butane	Butylene	Pentane	Pentene	Coke
Experimental value	4.22	1.39	13.10	2.49	37.83	9.51	5.92	6.08	2.67	6.47
Model predicted data	4.00	1.40	13.20	2.45	37.30	9.46	6.00	5.93	2.70	6.54

4.3. Profiles of chemical species and reaction temperature

As mentioned in Fig. 5a, methanol was consumed sharply at the first steps of the MTP reaction while producing higher olefins ($C_4^=, C_5^=, C_6^=$ and $C_7^=$) via the high rate reactions of methanol dehydration to heavy olefins (the 1st, 2nd, 3rd, and 4th reactions).

Moreover, a small amount of methanol was converted to methane and coke (12th reaction). It was remarkable that, after 100 s of the MTP reaction procedure, the rate of methanol conversion gradually declined, which is probably because of the initiation of the catalyst deactivation by means of coke formation. The coke deposition causes partial or complete pore blockings of the catalyst, which decreases the number of available active sites [26]. Methanol was almost thoroughly converted at 2000 s of time on stream. Corresponding with Fig. 5a, Fig. 5b represents that the methanol molar flux was high only at the entrance of the reactor and was almost completely converted to the MTP different products at the other sections of the reactor methanol.
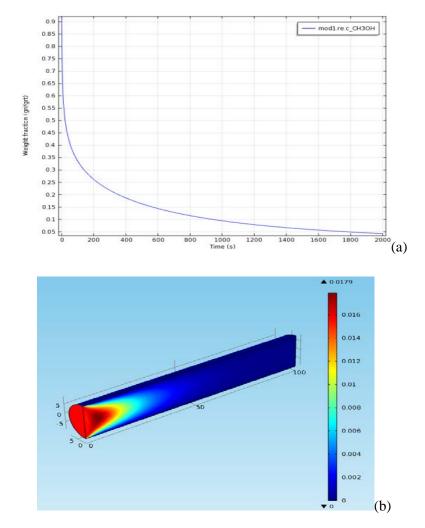

(a)

(b)

Figure 5. (a) The profile of methanol conversion in the MTP reactor versus time on stream predicted by CFD modeling; (b) The distribution of molar flux ($mol.m^{-2}.s^{-1}$) of methanol in the MTP reactor predicted by CFD modeling.

According to Fig. 6, the coke chemical species, which caused the catalyst deactivation, was produced unwantedly. Although the weight fraction of coke was negligible at the first steps of the MTP reaction particularly in our lab scale reactor, it gradually increased at the proceeding time, as shown in Fig. 6. The coke deposition causes a lot of disasters in industrial reactors; therefore, regeneration of the deactivated catalyst is inevitable.
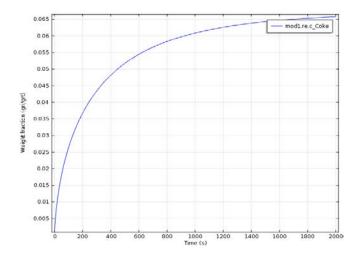
Figure 6. The Profile of coke formation versus time on stream predicted by CFD modeling.

As illustrated in Fig. 7, the production rates of propylene, ethylene, and pentene were sharp until 200 s time on stream; however, after that time, their generation rates decreased probably due to catalyst deactivation by coke generation. The weight fraction of butylene had a maximum point at 100th s and, then, it was reduced slowly because the generated butylene was consumed through the methylation reaction (the 5th reaction) to form the higher olefins. The weight fraction of propylene was greater than that of ethylene at the beginning to the end of the process, which was the characteristic point of the MTP reaction.
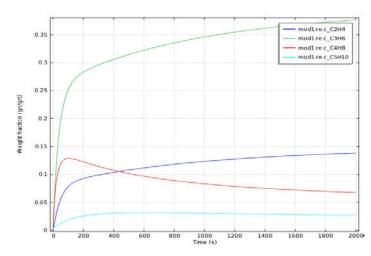

Figure 7. The profile of olefins weight fractions versus time on stream predicted by CFD modeling.

During the MTP reaction, few proportions of paraffins or alkanes, including ethane, propane, butane, and pentane, were generated. Fig. 8 represents the formation profiles of alkanes. The production procedures of all alkanes were similar. As evidenced by Fig. 8, the weight fractions of alkanes increased by reaction proceedings until 140 s of time on stream; then, the generation rate of alkanes was achieved in a steady-state condition. According to the proposed reaction mechanism, the alkanes were produced as a result of the 12th, 13th, 14th, 15th, and 16th reactions without any consumption in the MTP reaction.
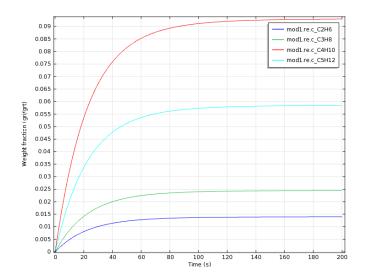
Figure 8. The profile of alkanes weight fractions versus time on stream predicted by CFD modeling.

The MTP reaction is a highly exothermic reaction; therefore, the solution of the energy equation is vital for recognizing the hot spots of the reactor. Needless to say, the hot spots unwantedly cause the catalyst deactivation by sintering the catalyst particles. Fig. 9 illustrates the temperature profile of the MTP reactor versus time on stream. The experimental reaction temperature was

regulated at 773.15 K. Since the MTP reaction was a highly exothermic reaction, the temperature increased to about 810 K, the temperature decreased steadily to about 804 K due to the endothermic property of the cracking reactions (the 8th, 9th, 10th, and 11th reactions), and then, the reactor temperature reached a steady-state condition.
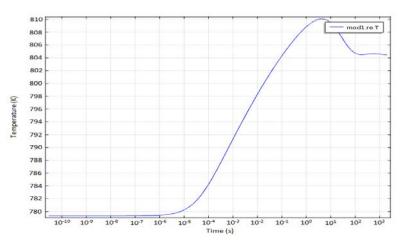

Figure 9. The temperature profile of the MTP reactor versus time on stream predicted by CFD modeling.

In order to compare the distributions of different chemical species, to distinguish the hydrodynamics of the reactive flows, and to investigate the reactor temperature, two reaction moments of 200 s and 2000 s were selected. Figures 10 and 11 show various

parameter distributions at the reaction moments of 200s and 2000 s, respectively. Figs. 10(a) and 10(b) illustrate the molar fluxes $(mol.m^{-2}.s^{-1})$ of propylene and ethylene, respectively. Propylene and ethylene were produced steadily along the

reactor, and their distributions were in parabolic shape. The propylene and ethylene were mainly generated in the outlet and center sections of the reactor. This was probably due to methanol dehydration to heavy as well as methylation reactions mainly occurring at the inlet section of the reactor. Consecutively, the cracking reactions which produced the light olefins of propylene and ethylene took place chiefly in the outlet and center sections of the reactor. Fig. 11(a) and Fig. 11(b) verify that the proportions of propylene and ethylene increase according to the time on stream, and the yield of propylene was greater than that of ethylene from the beginning to the end of the reaction. Figs. 10(c) and 10(d) show the molar fluxes of hexene and heptene, respectively. At the first 200 s of the reaction, the hexene and heptene were formed by methanol dehydration and methylation reactions; hence, the amounts of these higher olefins were enlarged during the first steps of the reaction. However, as evidenced by Fig. 11(c) and Fig. 11(d), in the later stages of the reaction, hexene and heptene underwent cracking to produce light olefins. Therefore, the molar fluxes of hexene and heptene were maximized on the first half of the reactor and, then, were gradually reduced in the outlet of the reactor. The reduction of heptene occurred sharply than that of hexene, since heptene was cracked to form alkanes and aromatics besides light olefins. The reactor's distributions of stream velocity (m.s^{-1}) are shown in Figures 10(e) and 11(e). According to Figures 10(e) and 11(e), it was inferred that velocity distribution was uniform along the reactor at various times on streams. The regime of the reacting flow is illustrated in Figures 10(f) and 11(f). These figures represented that the regime of the reacting flow was laminar, and the Reynolds number (Re No.) of the reactor center was greater than that of the wall sides of the reactor due to no-slip boundary condition. Comparing the Fig. 10(f) with Fig. 11(f), one finds out that the regime of the reacting flow did not considerably change during the reaction proceeding. Figures 10(g) and 11(g) represent variations of reactor temperature. According to Fig. 10(g) and due to the heat sinking of the reactor wall [11], the temperature was high in the center of the reactor and low on walls. At the first steps of the methanol conversion, the reaction took place chiefly near the inlet of the reactor. Since the MTP reaction was a highly exothermic reaction, the hot spots were found near the reactor inlet. Comparing Fig. 10(g) with Fig. 11(g), one may conclude that the reactor temperature at 2000 s was slightly lower than that at 200 s of time on stream. It was attributed to the partial deactivation of the catalyst at 2000 s of time on stream which caused the lower methanol conversion. Consequently, the heat released from the exothermic MTP reaction reduced and caused the lower reactor temperature. Moreover, by the catalyst deactivation progressing, the hot spots location transferred to the reactor outlet. The reason is explained as follows:

By continuing the catalyst deactivation, the amount of coke was increased and the coke chemical species were propagated from the reactor inlet to its outlet [11]. This issue deteriorated the MTP reaction at the reactor inlet and accelerated the reaction at the reactor outlet where the catalyst was not thoroughly deactivated. Accordingly, the hot spots were carried to the reactor outlet.
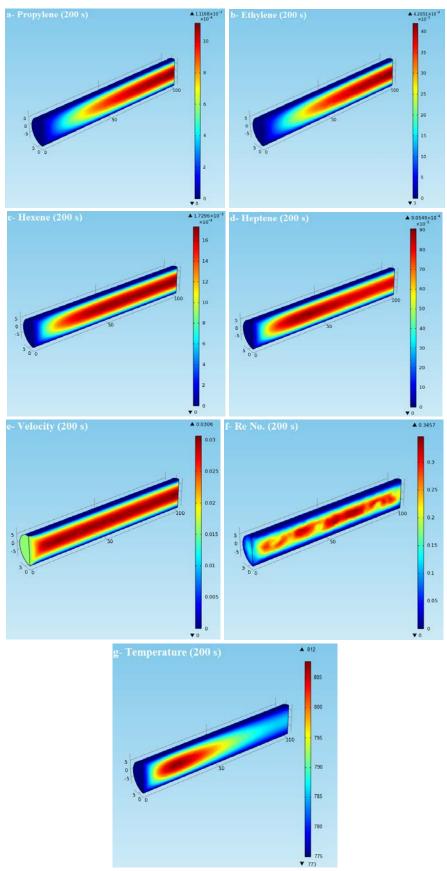
Figure 10. The parameters distribution at time on stream of 200 s; molar fluxes (mol.m^{-2}.s^{-1}) of a) propylene; b) ethylene; c) hexene; d) heptene; e) velocity distribution (m.s^{-1}); f) value of Reynolds number in the reactor; g) reactor temperature (K).
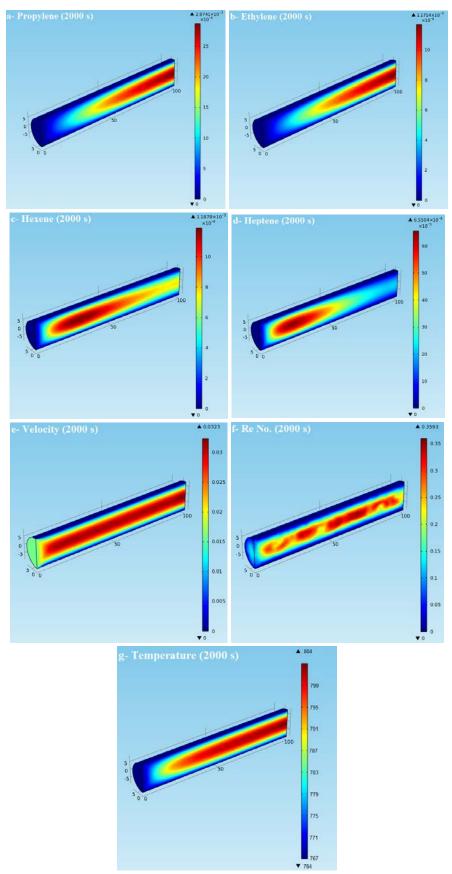
Figure 11. The parameters distribution at time on stream of 2000 s; molar fluxes (mol.m^{-2}.s^{-1}) of a) propylene; b) ethylene; c) hexene; d) heptene; e) velocity distribution (m.s^{-1}); f) value of Reynolds number in the reactor; g) reactor temperature (K).

5. Conclusions

A detailed reaction mechanism and kinetic model based on the hydrocarbon pool theory and the conjugate methylation/cracking mechanisms were coupled with the CFD model. The purpose of CFD modeling was to simulate the kinetics, hydrodynamics, and energy equation of the MTP process based on the experimental data obtained over the H-MnAlMFI catalyst. The experimental data were obtained under the optimal operating conditions. The CFD modeling of the MTP reaction was also carried out under the optimal operating conditions. The profiles of different chemical species were achieved by CFD modeling, and good agreement was observed between the experimental data and the model predicted values.

References

[1] Hadi, N., Niaei, A., Nabavi, S. R. and Farzi, A., "Kinetic study of methanol to propylene process on high silica H-ZSM5 catalyst", *Iranian J. Chem. Eng.*, **10** (4), 16 (2013).

[2] Hadi, N., Niaei, A., Nabavi, S. R., Alizadeh, R., Shirazi, M. N. and Izadkhah, B., "An intelligent approach to design and optimization of M-Mn/H-ZSM-5 (M: Ce, Cr, Fe, Ni) catalysts in conversion of methanol to propylene", *J. Taiwan Inst. Chem. Eng.*, **59**, 173 (2016).

[3] Hadi, N., Niaei, A., Nabavi, S. R., Farzi, A. and Shirazi, M. N., "Development of a new kinetic model for methanol to propylene process on Mn/H-ZSM-5 catalyst", *Chem. Biochem. Eng. Q.*, **28**, 53 (2014).

[4] Rostamizadeh, M. and Taeb, A., "Highly selective Me-ZSM-5 catalyst for methanol to propylene (MTP)", *J. Ind. Eng. Chem.*, **27**, 297 (2015).

[5] Guo, W., Xiao, W. and Luo, M., "Comparison among monolithic and randomly packed reactors for the methanol-to-propylene process", *Chem. Eng. J.*, **207**, 734 (2012).

[6] Guo, W., Wu, W., Luo, M. and Xiao, W., "Modeling of diffusion and reaction in monolithic catalysts for the methanol-to-propylene process", *Fuel Process. Technol.*, **108**, 133 (2013).

[7] Alwahabi, S. M. and Froment, G. F., "Conceptual reactor design for the methanol-to-olefins process on SAPO-34", *Ind. Eng. Chem. Res.*, **43**, 5112 (2004).

[8] Schoenfelder, H., Hinderer, J., Werther, J. and Keil, F. J., "Methanol to olefins: Prediction of the performance of a circulating fluidized-bed reactor on the basis of kinetic experiments in a fixed-bed reactor", *Chem. Eng. Sci.*, **49**, 5377 (1994).

[9] Soundararajan, S., Dalai, A. and Berruti, F., "Modeling of methanol to olefins (MTO) process in a circulating fluidized bed reactor", *Fuel*, **80**, 1187 (2001).

[10] Chang, J., Zhang, K., Chen, H., Yang, Y. and Zhang, L., "CFD modelling of the hydrodynamics and kinetic reactions in a fluidised-bed MTO reactor", *Chem. Eng. Res. Des.*, **91**, 2355 (2013).

[11] Zhuang, Y. Q., Gao, X., Zhu, Y. P. and Luo, Z. H., "CFD modeling of methanol to olefins process in a fixed-bed reactor", *Powder Technol.*, **221**, 419 (2012).

[12] Zhu, L. T., Xie, L., Xiao, J. and Luo, Z. H., "Filtered model for the cold-model gas-solid flow in a large-scale MTO fluidized bed reactor", *Chem. Eng. Sci.*, **143**, 369 (2016).

[13] Lu, B., Luo, H., Li, H., Wang, W., Ye, M., Liu, Z. and Li, J., "Speeding up CFD

simulation of fluidized bed reactor for MTO by coupling CRE model", *Chem. Eng. Sci.*, **143**, 341 (2016).

[14] Nijemeisland, M. and Dixon, A. G., "CFD study of fluid flow and wall heat transfer in a fixed bed of spheres", *AIChE J.*, **50**, 906 (2004).

[15] Ding, J. and Gidaspow, D., "A bubbling fluidization model using kinetic theory of granular flow", *AIChE J.*, **36**, 523 (1990).

[16] Tian, Z. F., Tu, J. Y. and Yeoh, G., "CFD studies of indoor airflow and contaminant particle transportation", *Particul. Sci. Technol.*, **25**, 555 (2007).

[17] Coussirat, M., Guardo, A., Mateos, B. and Egusquiza, E.,"Performance of stress transport models in the prediction of particle to fluid heat transfer in packed beds", *Chem. Eng. Sci.*, **62**, 6897 (2007).

[18] Salari, D., Niaei, A., Yazdi, P. C. and Derakhshani, M., "CFD flow and heat transfer simulation for empty and packed fixed bed reactor in catalytic cracking of naphtha", *Int. J. Chem. Biol. Eng.*, **1**, 50 (2008).

[19] Shahhosseini, S., Alinia, S. and Irani, M., "CFD simulation of fixed bed reactor in fischer-tropsch synthesis of GTL technology", Proceeding of *The World Academy of Science Engineering and Technology,* World Academy Science Publications, Berlin, Germany, **1**, pp. 585-589 (2009).

[20] Guardo, A., Coussirat, M., Recasens, F., Larrayoz, M. and Escaler, X., "CFD study on particle-to-fluid heat transfer in fixed bed reactors: Convective heat transfer at low and high pressure", *Chem. Eng. Sci.*, **61**, 4341 (2006).

[21] Jin, Y., Asaoka, S., Zhang, S., Li, P. and Zhao, S., "Reexamination on transition-metal substituted MFI zeolites for catalytic conversion of methanol into light olefins", *Fuel Process. Technol.*, **115**, 34 (2013).

[22] Kim, Y., Kim, J. C., Jo, C., Kim, T. W., Kim, C. U., Jeong, S. Y. and Chae, H. J., "Structural and physicochemical effects of MFI zeolite nanosheets for the selective synthesis of propylene from methanol", *Microporous Mesoporous Mater.*, **222**, 1 (2015).

[23] Hadi, N., Niaei, A., Nabavi, S. R., Shirazi, M. N. and Alizadeh, R., "Effect of second metal on the selectivity of Mn/H-ZSM-5 catalyst in methanol to propylene process", *J. Ind. Eng. Chem.*, **29**, 52 (2015).

[24] Hadi, N., Alizadeh, R. and Niaei, A., "Selective production of propylene from methanol over nanosheets of metal-substituted MFI zeolites", *J. Ind. Eng. Chem.*, In press, (2017).

[25] Treacy, M. M. and Higgins, J. B., Collection of simulated XRD powder patterns for zeolites, 5th Revised Ed., Elsevier, (2007).

[26] Alwahabi, S. M. and Froment, G. F., "Single event kinetic modeling of the methanol-to-olefins process on SAPO-34", *Ind. Eng. Chem. Res.*, **43**, 5098 (2004).